



OPEN ACCESS

EDITED BY

Alessandro Polini,
Institute of Nanotechnology (CNR), Italy

REVIEWED BY

Madhuri Dey,
Strand Therapeutics, Inc., United States
Paola Ginestra,
University of Brescia, Italy

*CORRESPONDENCE

Cristina Scielzo,
✉ scielzo.cristina@hsr.it
Silvia Farè,
✉ silvia.fare@polimi.it

SPECIALTY SECTION

This article was submitted to Bioinspired and Complex Materials, a section of the journal Frontiers in Biomaterials Science

RECEIVED 26 October 2022

ACCEPTED 02 January 2023

PUBLISHED 13 February 2023

CITATION

Ribezzi D, Pinos R, Bonetti L, Cellani M, Barboglio F, Scielzo C and Farè S (2023), Design of a novel bioink suitable for the 3D printing of lymphoid cells. *Front. Front. Biomater. Sci.* 2:1081065. doi: 10.3389/fbiom.2023.1081065

COPYRIGHT

© 2023 Ribezzi, Pinos, Bonetti, Cellani, Barboglio, Scielzo and Farè. This is an open-access article distributed under the terms of the [Creative Commons Attribution License \(CC BY\)](https://creativecommons.org/licenses/by/4.0/). The use, distribution or reproduction in other forums is permitted, provided the original author(s) and the copyright owner(s) are credited and that the original publication in this journal is cited, in accordance with accepted academic practice. No use, distribution or reproduction is permitted which does not comply with these terms.

Design of a novel bioink suitable for the 3D printing of lymphoid cells

Davide Ribezzi¹, Riccardo Pinos², Lorenzo Bonetti¹, Marco Cellani², Federica Barboglio², Cristina Scielzo^{2*} and Silvia Farè^{1*}

¹Department of Chemistry, Materials and Chemical Engineering, Politecnico di Milano, Milano, Italy, ²Unit of Malignant B cells Biology and 3D Modelling, Division of Experimental Oncology, IRCCS Ospedale San Raffaele, Milano, Italy

Introduction: For decades, *in vitro* 2D cell culture techniques have been employed in research, but they fail to recapitulate the complexity of natural tissues. 3D bioprinting could potentially overcome this drawback due to the possibility to control the spatial disposition of living cells and the geometry of the 3D scaffold.

Materials and methods: This study reports the design and characterization of a novel bioink for extrusion bioprinting, analyzing different blend formulations composed of alginate, gelatin, and methylcellulose, suitable as cell-laden bioink for lymphoid cells, in particular those isolated from patients with Chronic Lymphocytic Leukemia (CLL). The rheological properties as a function of temperature and the printability of the formulations were investigated to define the optimal printing parameters. *In vitro* stability of the printed scaffolds was investigated under culture conditions and compression tests were performed on printed and bioprinted scaffolds to compare their mechanical properties with those of fresh lymphoid tissue. Finally, MEC1, a CLL cell line, was bioprinted to investigate cell viability, cell density, and cell capability to be released from the scaffold over time.

Results and discussion: Results showed that, for the selected blends, good shape fidelity and printing accuracy were achieved with a limitation on the number of printed layers. Scaffolds withstood culture conditions showing stability for up to 3 weeks and their mechanical properties were similar to those of lymphoid tissues already reported in the literature. High cell viability after 21 days was observed for both MEC1 and primary peripheral mononuclear cells, confirming the possibility to use the selected formulation to successfully bioprint lymphoid cells by possibly mimicking their native lymphoid microenvironment.

KEYWORDS

3D bioprinting, bioink, chronic lymphocytic leukemia, 3D culture, lymphoid cells

1 Introduction

In vitro cell culture is fundamental for many biomedical studies including cell biology, pathology, genetics, tissue engineering, and drug development (Meyvantsson and Beebe, 2008). 2D cell culture techniques have been used for decades leading to major discoveries and understanding of human biology and disease (Lee et al., 2008; Thayer et al., 2020). They represent a simple, efficient, and affordable approach using 2D surfaces, such as modified polystyrene well plates, flasks, and Petri dishes, which allow homogeneous access to nutrients and growth factors. However, 2D cell cultures fail to recapitulate the complexity of physiological tissues, where nearly all cells reside in a 3D microenvironment composed of vasculature enabling oxygen and nutrients supply as well as cell-cell communications, cell-extracellular matrix (ECM) interactions, and metabolic waste removal (Young and Beebe, 2010).

For the design and preparation of complex 3D structures as *in vitro* models, biofabrication is becoming a more and more prominent field, combining the principles of engineering with

living cells, biomaterials, and bioactive molecules (Moroni et al., 2018). Among possible strategies (Moroni et al., 2018), extrusion-based bioprinting, using different extrusion methods, i.e., pneumatic or mechanical (*via* piston- or screw-driven systems), is rapidly becoming an established approach due to the possibility of easily printing multiple materials, the relatively low cost, and fast access to the required hardware for this technology (Ribeiro et al., 2017). A critical step in this process involves the formation of printed filaments, which constitute the basic building block in extrusion-based bioprinting (Jungst et al., 2016). Therefore, the selection of the adequate biomaterial to be used as bioink or as biomaterial-ink (Malda et al., 2013) is a crucial factor, which relies on several variables. The selection of biomaterials inks used to print acellular structures, on which cells are seeded or that can also be used as support for the whole model, focuses mainly on the rheological properties. Ideally, the biomaterial ink should show a shear-thinning behavior (i.e., the viscosity decreases by increasing the shear rate), yield stress, and quick recovery kinetics, thus behaving as a non-viscous fluid during extrusion and as a stable gel after printing (Malda et al., 2013; Jungst et al., 2016). In addition to these properties, bioinks require the printing process to ensure the viability of the embedded cells, therefore they are generally aqueous formulations with tuned rheological properties that can provide a highly hydrated environment for the encapsulated cells (Levato et al., 2020). For this reason, hydrogel precursors that can be crosslinked pre-, during, or post-the bioprinting process are often exploited, but a good shape fidelity after printing is a crucial characteristic as well. For this reason, an appropriate biofabrication window, which relates the shape fidelity to the crosslinking density/stiffness of the hydrogel has to be considered (Levato et al., 2020).

Among several fields of applications, 3D bioprinting has found widespread use in experimental oncology research (Datta et al., 2020), in particular to mimic the complexity of the 3D tumor microenvironment for the development of appropriate *in vitro* models (Langer et al., 2019). For many years, even cancer pathophysiology studies and drug testing have relied on conventional 2D *in vitro* culture systems and *in vivo* animal models (Yamada and Cukierman, 2007). Although widely used, these models have many limitations, thus poorly reflecting the *in vivo* environment as well. Recently, *in vitro* 3D models, mainly focusing on solid tumors mimicking specialized microenvironments, based on advanced biomaterials and microfluidics, have helped to elucidate new mechanisms and potential therapeutic targets that could not otherwise be studied in conventional 2D *in vitro* cultures (Langer et al., 2019). 3D systems have also been applied to the study of hematological cancers, in particular for Chronic Lymphocytic Leukemia (CLL) (Sbrana et al., 2021) where the tissue microenvironment has a fundamental role in the development, progression, and response to therapy (Scielzo and Ghia, 2020). CLL cells circulate between the peripheral blood, lymphoid organs, and bone marrow, thus making this neoplasm highly dependent on signals and stimuli from the microenvironment. For this reason, the cross-talk with the surrounding environment in promoting the proliferation and survival of CLL cells has been central to the development of new and targeted treatments, reviewing how the disease is managed from the clinical point of view (Burger, 2012).

In this study, we report the design and characterization of new natural polymer-based bioink formulations for extrusion-based bioprinting, that allowed to successfully bioprint healthy and leukemic lymphocytes, in particular, CLL cells and primary peripheral mononuclear cells. We successfully optimized the printing process and the procedures to perform the analysis

TABLE 1 Different compositions of the blend formulations.

	3A1M	2A2M	1A3M	0A4M
MC 2% w/v	1	2	3	4
Gel 10% w/v	1	1	1	1
Alg 2% w/v	3	2	1	0

starting from mechanical and physio-chemical evaluations of the different formulations. Our results demonstrate that with our bioink we can efficiently 3D bioprint lymphoid cells and keep them in culture for up to 21 days, therefore establishing a long-term 3D culture model for lymphoid cells.

2 Materials and methods

2.1 Hydrogel preparation

Methylcellulose (M0512, viscosity 4,000 cP, 2% in aqueous solution at 20°C), alginate sodium salt (A0682, 15–25 cP, 1% in aqueous solution), and type A gelatin derived from porcine skin (G1890, gel strength ~300 g Bloom) were obtained from Sigma-Aldrich. Methylcellulose (MC), gelatin (Gel), and alginate (Alg) powders were dissolved in Hank's Balanced Salt Solution (HBSS), obtaining 2%, 10%, and 2% w/v solutions, respectively (Chung et al., 2013).

Different blends were prepared by mixing the previously obtained solutions, varying the volume ratios (in mL) for each component (Table 1). Finally, 0.1 M CaCl₂ crosslinking solution was prepared by mixing 5 mL of 1 M CaCl₂ (VWR Life Science Biotechnology) with 45 mL of HBSS. Hydrogels were immersed in the solution for the crosslinking process for 10 min.

2.2 Rheological characterization

The rheological properties of the different formulations (Table 1) were investigated to identify the gelation point and the optimal printing temperature. Rheological tests were performed using a rheometer (MCR 302, Anton Paar) equipped with parallel plate geometry ($\varnothing = 25$ mm, working gap 1 mm).

Preliminary amplitude sweep tests were carried out on each formulation (Table 1) to identify the linear viscoelastic region (LVR) by applying an oscillatory strain (γ) in the 0.01%–10% range, setting a 1 Hz frequency (ν), at 4°C and 40°C. Then, to identify the transition temperature of Gel and MC (i.e., $T_{gel-sol}$ and $T_{sol-gel}$), temperature sweep tests were carried out in the 5°C–60°C range, with a heating ramp of 2°C/min, $\gamma = 0.05\%$, $\nu = 1$ Hz. The transition temperatures were identified from the storage (G') and loss moduli (G'') as the crossover point ($G' = G''$) (Desbrières et al., 2000).

2.3 Shape fidelity

2.3.1 Spreading ratio

Three straight lines were designed in Fusion 360 (Autodesk) and imported in HeartWare setting their width at 250 μ m, corresponding

to the dimension of the printing nozzle (25 G). The formulations were extruded using a BIO X 3D bioprinter (CELLINK AB, Gothenburg, Sweden), with a printing pressure of 17 kPa, previously investigated through the filament characterization test, and different printing speeds ($v = 3, 5, 7, 9, 11$ mm/s), at 15°C and 25°C. Images were acquired with an optical microscope (DMi1, Leica) and Fiji ImageJ software was used to outline and measure (Supplementary Figure S1A) the width of the printed strands. The spreading ratio was calculated as described in Eq. 1:

$$\text{Spreading Ratio} = \frac{w_i}{w_0} \quad (1)$$

where w_i and w_0 refer to the printed strand width and the theoretical strand width, respectively. Measurements were performed on 5 different points of the same filament (Supplementary Figure S1A) and the mean value was calculated. The mean value of the spreading ratio of the 3 filaments was finally obtained.

2.3.2 Printing accuracy

Two concentric squares ($l = 10$ mm and $l = 5$ mm, respectively for the outer and the inner one) were designed in Fusion360 (Autodesk) and imported into HeartWare software (Supplementary Figure S1B). For each formulation, 3 structures were printed at 10 mm/s printing speed, 17 kPa printing pressure, at 15°C and 25°C. Images were acquired with a 13 MP (resolution: 4160 × 3120) phone camera and Fiji ImageJ software was used to measure the area of the inner and the outer squares. The printing accuracy (%) was calculated as described by Eq. 2 (Giuseppe et al., 2018) for both the inner and the outer squares:

$$\text{Printing Accuracy} [\%] = \left[1 - \left(\frac{|A_i - A|}{A} \right) \right] * 100 \quad (2)$$

where A_i and A refer to the mean area of the printed squares and the mean area of the CAD design, respectively. The mean value of printing accuracy for the inner and outer squares was obtained for each of the three printed structures.

2.3.3 Uniformity factor

Shape fidelity was also investigated using a 2 × 3 grid designed in Fusion360 (Autodesk) and imported into HeartWare software to set the filament width at 250 μm (Supplementary Figure S1C). Hydrogels were printed at 10 mm/s printing speed, 17 kPa printing pressure, at 15°C and 25°C.

Images were acquired with a 13 MP (resolution: 4160 × 3120) phone camera and Fiji ImageJ software was used to outline and measure the perimeter and the area of the pores of the printed grids, using “Freehand selection” and “Polygon selection” functions (Supplementary Figure S1C). For each method, 4 measurements were performed on 4 different pores of the grid. The mean value and the standard deviation were obtained. The uniformity factor (Pr) was then obtained for each printed hydrogel as described in Eq. 3 (Ouyang et al., 2016; Schwab et al., 2020):

$$\text{Pr} = \frac{(\text{pore perimeter})^2}{16 * \text{pore area}} \quad (3)$$

The Pr parameter was used to compare the printing accuracy of the printed pores to the designed square pores; a final value deviating from 1 was set as the threshold for a non-accurate printing of the material (Soltan et al., 2019).

2.4 Compressive mechanical properties characterization

The compressive mechanical properties of the printed samples ($n = 3$ per formulation) were tested by Dynamic Mechanical Analyzer (DMA Q800, TA Instruments), equipped with compression clamps. Tests were carried out at 37°C, applying a preload of 0.001 N. A strain-controlled ramp was applied at 1%/min rate down to −30% strain, then an unload phase was applied at 5%/min rate up to 1% strain. The considered compressive mechanical parameters were the elastic modulus (E, measured as the slope in the 0%–2% strain range), the stiffness (K, measured as the slope in the 5%–15% strain range), the maximum stress (σ_{\max}), and the residual deformation (ϵ_{res}).

2.5 Stability evaluation

To investigate the stability of the hydrogel formulations over time, a weight variation test at 37°C was performed in DMEM culture medium for bulk, printed scaffolds, and bioprinted constructs. The specimens ($n = 4$) were first weighted and subsequently immersed in 3 mL of culture medium. The weight at different time points (up to 21 days) was then recorded. At each timepoint, the incubation fluid was totally removed and 3 mL of fresh culture medium were added after weighing the hydrogel samples (Contessi Negrini et al., 2018). The percentage of weight variation was obtained from Eq. 4:

$$\Delta W [\%] = \frac{W_t - W_0}{W_0} * 100 \quad (4)$$

where W_t and W_0 refer to the weight at each timepoint and the weight at $t = 0$, respectively.

The detection of MC in the polymeric blend and its release over time were qualitatively investigated keeping the hydrogels at 37°C in DMEM culture medium for up to 21 days. The printed structures were stained by adding chlorine–zinc–iodine solution (Carl Roth, Karlsruhe, Germany) dropwise to the scaffolds immediately after printing (Schütz et al., 2017). At different time points, the release of MC was qualitatively checked, evaluating the change in the hydrogel color.

2.6 In vitro biological tests

For the *in vitro* biological characterization, the hydrogels (Par. 2.1) were prepared in sterile conditions, after UV sterilizing the polymer powders (30 min).

2.6.1 Selected cell types

MEC1 cell line, previously expanded from a patient with CLL (Stacchini et al., 1999), was obtained from Deutsche Sammlung von Mikroorganismen und Zellkulturen GmbH and cultured in RPMI 1640 medium (EuroClone, Pero, Italy) supplemented with 10% v/v Fetal Bovine Serum (FBS) and 15 mg/mL gentamicin, at 37°C and 5% CO₂.

Peripheral mononuclear cells were isolated with ficoll gradient from Buffy coats under the approved protocol Leu-Buffy coat by the Ospedale San Raffaele (OSR, Milan, Italy) ethics committee under the research “Characterization of leukocyte subpopulations from buffy coats.”

2.6.2 Cell bioprinting

MEC1 or primary peripheral mononuclear cells were counted, centrifuged at 1500 RPM for 5 min, and then gently mixed with the

optimized hydrogel formulation using two Luer lock syringes in a 1:10 medium:hydrogel ratio (Sbrana et al., 2021). The bioink was then loaded in a 3 mL cartridge and placed in the extrusion-based BIO X 3D bioprinter (CELLINK AB, Gothenburg, Sweden). The 3D scaffolds ($5 \times 5 \times 1 \text{ mm}^3$) were designed with Fusion 360 (Autodesk). A 25 G nozzle was used to print the structures and the constructs (30% infill density, rectilinear pattern) directly in a multiwell plate at 5 mm/s speed and a pressure range, depending on cell concentration, of 20–25 kPa. The obtained constructs were crosslinked for 10 min with 0.1 M CaCl_2 directly in the well plate and cultured in RPMI 1640 medium (EuroClone, Pero, Italy), supplemented with 10% FBS and 15 mg/mL gentamicin (Lonza, Basel, Switzerland), at 37°C, 5% CO_2 up to 21 days.

Embedded cells were imaged by Leica DMi1 optical microscope at different time points to qualitatively assess their viability, up to 21 days.

Compressive mechanical tests were performed at selected timepoints ($t = 0, 7, 21$ days) to investigate the influence of the metabolic activity of the embedded cells on the mechanical behavior of the bioprinted scaffolds. Tests were performed as previously described (Par. 2.4).

2.6.3 Live/dead assay

Cell viability was analyzed at different time points ($t = 2, 7, 10, 14, 21$ days) using the LIVE/DEAD[®] Cell Imaging Kit (Thermo Fisher Scientific). The constructs ($n = 1$ for each blend) were washed for 30 min with DMEM without serum (Thermo Fisher Scientific), and LIVE/DEAD[®] kit was added in a 1:3 ratio. After 1 h of incubation at 37°C, 5% CO_2 , the constructs were washed again with medium without serum and observed with the fluorescent microscope (AXIO Observer Z1) using FITC and TRITC light filters, respectively for live (green) and dead (red) cells. Three images per sample were acquired along the scaffold thickness (z -axis) at different magnifications (5, 10, and 20x).

2.6.4 Alamar blue assay

In parallel, cellular metabolic activity was analyzed at different time points ($t = 2, 7, 10, 14, 21$ days) using the AlamarBlue[®] assay (Thermo Fisher Scientific, Massachusetts, United States) on the bioprinted constructs. The reagent was mixed with the appropriate medium (RPMI 1640 complete medium) in a 1:10 ratio, respectively; then, 1 mL of the mix was added to each well. As assay blank, RPMI complete medium with a 3D bioprinted scaffold without embedded cells was used. After 24 h of incubation at 37°C, 5% CO_2 , 100 μL of the mix were collected and transferred to a 96-well white plate and the fluorescence values were read ($\lambda_{\text{ex}} = 560 \text{ nm}$; $\lambda_{\text{em}} = 590 \text{ nm}$) using a spectrophotometer (Victor, Perkin Elmer).

2.7 Statistical analysis

Student's t -test was performed for statistical analysis (GraphPad Prism v.9.0a). Unpaired t -test was used for parametric comparisons of data sets ($*p < 0.05$).

3 Results

3.1 Hydrogel design

All the formulations were successfully prepared according to the described protocol. However, A04M qualitatively exhibited a low

consistency due to the absence of alginate in the blend that allowed for the formation of the crosslinked network in the other formulations. For this reason, it was not considered for further characterization.

3.2 Rheological properties and printability optimization

In this study, the rheological properties of different hydrogel formulations (3A1M, 2A2M, and 1A3M, Table 1) were assessed by strain sweep and temperature sweep tests.

Strain sweep analyses (Supplementary Figure S2A) were carried out at 4°C and 40°C to identify the LVR of all the hydrogel formulations. The temperatures were selected considering the thermal transition behavior of Gel and MC: 4°C $\ll T_{\text{gel-sol}}$ of Gel ($T_{\text{gel-sol}} = 34^\circ\text{C}$ – 35°C , Figure 1B) and 40°C $> T_{\text{sol-gel}}$ of MC ($T_{\text{sol-gel}} = 37^\circ\text{C}$ – 40°C , Figure 1B), as detected by the rheological tests in temperature sweep. For the following characterization, the limit of the LVR was set at $\gamma = 0.05\%$ for all the specimens.

Temperature sweep tests were carried out to study the viscoelastic behavior of the three formulations as a function of temperature. The obtained curves (Figures 1A, B; Supplementary Figure S2B) displayed a similar trend: at low temperatures, $G' > G''$ indicating that the specimens are in a gel-like state, behaving as solid viscoelastic materials (Borzacchiello et al., 2017). Then, an evident drop in the viscoelastic parameters occurs, accompanied by the crossover between G' and G'' (i.e., $G' = G''$), ascribable to the gel-sol transition of gelatin in the blend (Ahmed, 2017). A further increase in temperature leads to a second crossover point between G' and G'' (Figure 2B), due to the sol-gel transition of methylcellulose in the blend (Coughlin et al., 2021). After this point, G' is higher than G'' until the end of the test, indicating a gel-like behavior of the different formulations.

As it is possible to observe in Figures 1A, B, a trend for G' can be detected: 1A3M $>$ 2A2M \geq 3A1M. Such a trend reflects the increase in the gel strength of the formulations, referable to the increased concentration of MC, widely recognized as a viscosity-enhancing additive (Nasatto et al., 2015).

For all the formulations, the transition temperatures (gel-sol and sol-gel, respectively for Gel and MC) were calculated from the crossover points of G' and G'' curves. The $T_{\text{gel-sol}}$ of Gel was found in the 34°C–35°C range, while the $T_{\text{sol-gel}}$ of MC was detected in the 37°C–40°C range. The transition temperatures detected shifted from the ones that can be found in the literature for pristine Gel [$T_{\text{gel-sol}} = 20^\circ\text{C}$ – 30°C (Van Hoorick et al., 2015)] and MC [$T_{\text{sol-gel}} = 55^\circ\text{C}$ – 60°C (Bonetti et al., 2021)] due to the synergistic effect of salts (HBSS) and other polymers in the blend (Bonetti et al., 2021).

A first printability characterization was performed to assess the printing pressure and to verify the actual formation of a filament following the extrusion of the hydrogel (O'Connell et al., 2020) (Supplementary Figure S2). In this way, it is possible to qualitatively evaluate whether the analyzed blends are printable and suitable for the fabrication of 3D structures. For all the extrusion trials, both 3A1M and 2A2M blends qualitatively showed a smooth and uniform filament, able to hang, reaching a length of more than 5 mm (Supplementary Figure S2C) applying a 17 kPa pressure for both formulations. On the other hand, 1A3M had a different behavior; in fact, in two trials (Supplementary Figure S2C) an irregular filament with a fractured-like, brittle morphology was evidenced, while in the third one a droplet morphology was observed at the nozzle tip

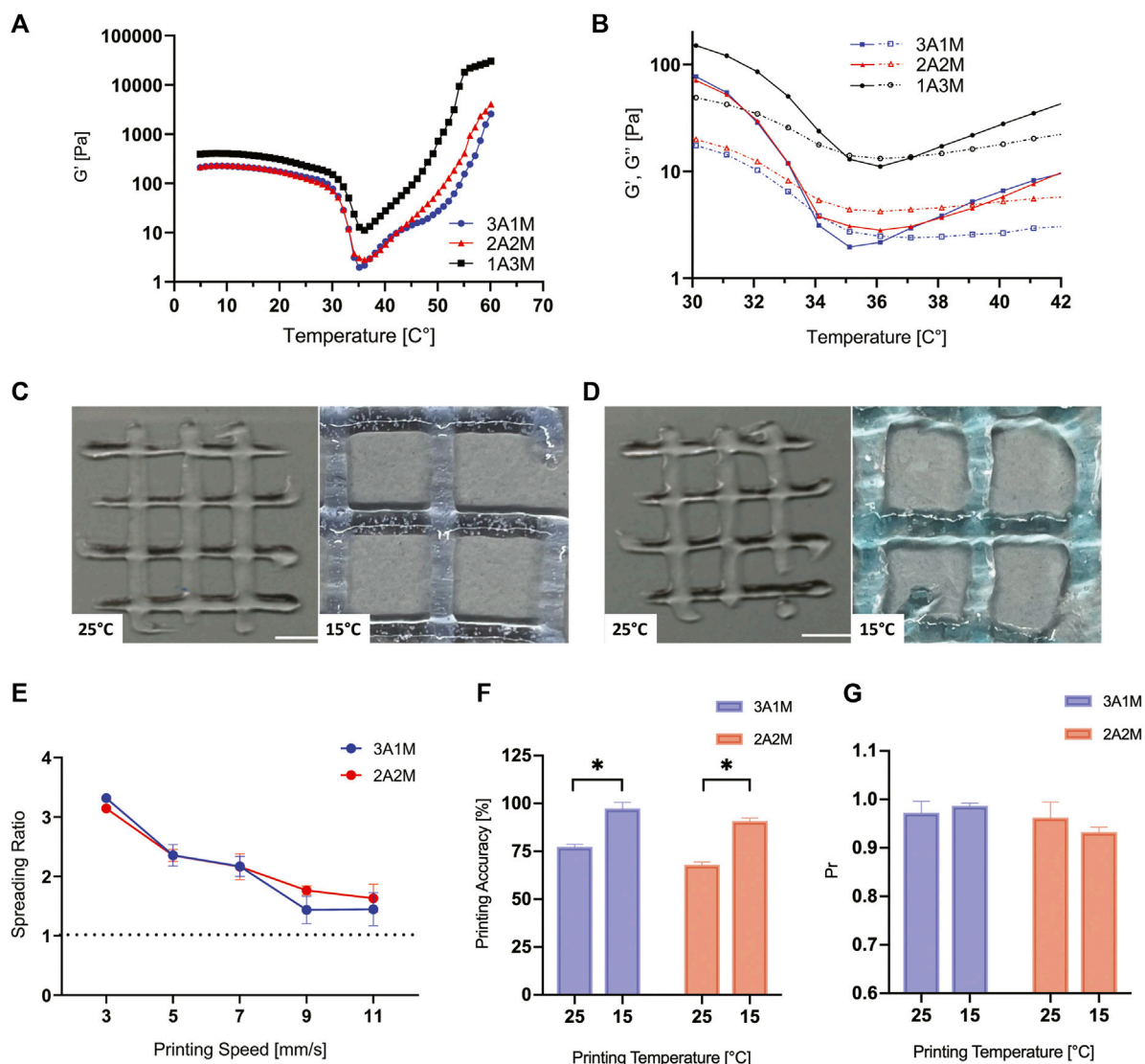


FIGURE 1

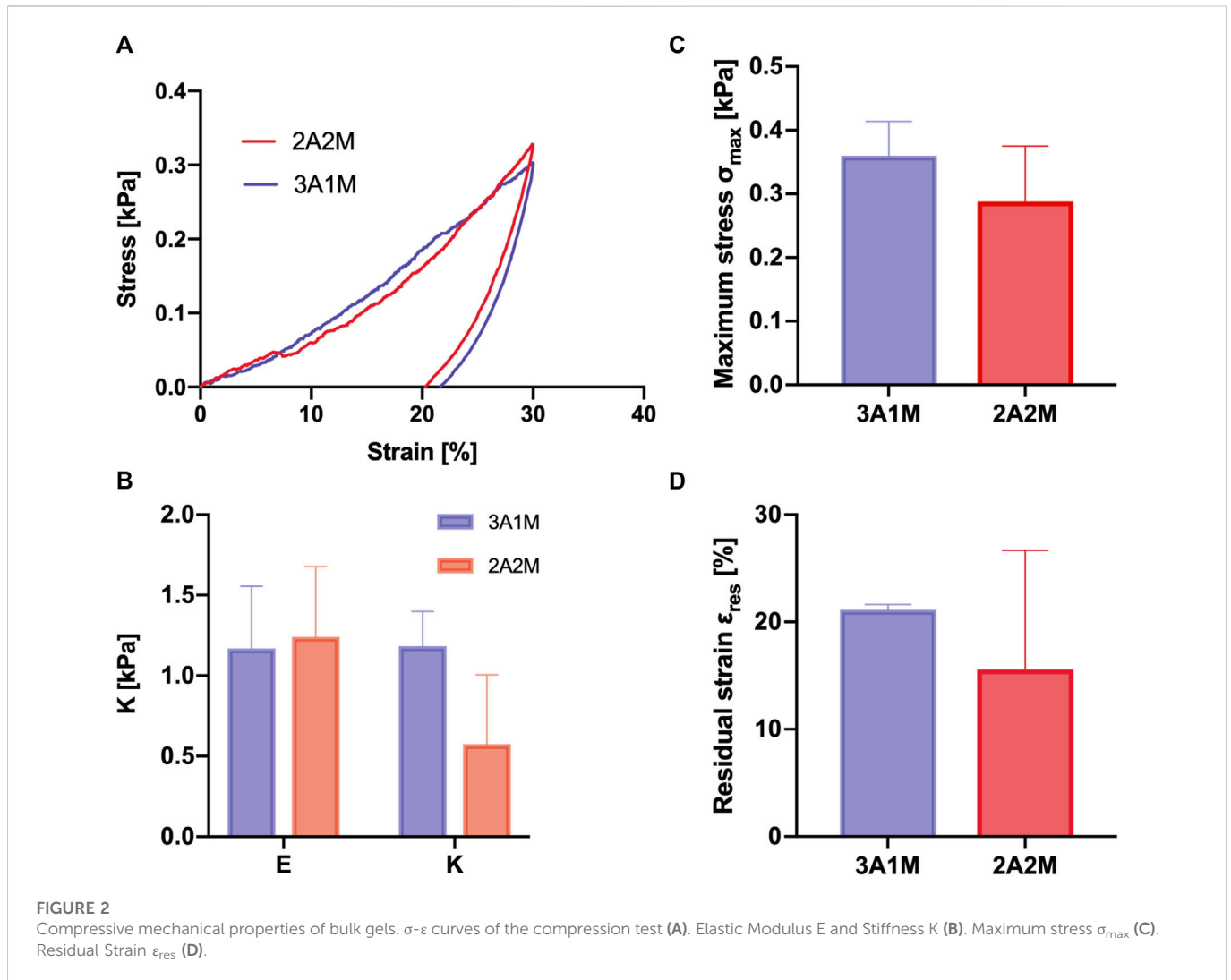
Rheological properties and printing parameters optimization. Temperature sweep tests performed to investigate the transition temperatures ($T_{gel-sol}$ and $T_{sol-gel}$) of 3A1M, 2A2M, and 1A3M hydrogels, reporting G' (Pa) vs. T ($^{\circ}\text{C}$) (A) and G' and G'' (Pa) vs. T ($^{\circ}\text{C}$) in the temperature range where the transition occurs (B). Representative printability tests performed on 3A1M (C) and 2A2M (D) hydrogels at 15 $^{\circ}\text{C}$ and 25 $^{\circ}\text{C}$ to investigate the printing accuracy. Spreading Ratio (E), Printing accuracy (%) (F), and Uniformity factor (G) values of the 3A1M and 2A2M formulations, comparing the results obtained at 15 $^{\circ}\text{C}$ and 25 $^{\circ}\text{C}$.

(Supplementary Figure S2C). 1A3M was printed with a 23 kPa pressure to possibly obtain a homogeneous printed strand.

Considering this preliminary qualitative test, further printability investigations were performed only on 3A1M and 2A2M blends, as the 1A3M blend was found inconsistent and unreliable according to the initial filament characterization.

The spreading ratio was calculated by Eq. 1. A low spreading ratio is desirable to allow the printing of structures with high shape fidelity. Hence, a value close to 1 is desired, as it would represent the optimal ratio between the printed filament diameter and the theoretical one (Schwab et al., 2020). Results have shown that the spreading ratio decreases as the printing speed increases (Figure 1E). According to these results, a printing speed between 9 and 11 mm/s provided the optimal value of the spreading ratio, which was close to 1 for the two blends, allowing the extruded strand to a lower spreading and collapse after the deposition.

The printing accuracy evaluation (Figures 1C, D, F) and the uniformity factor (Figure 1G) investigation were performed at 25 $^{\circ}\text{C}$ and 15 $^{\circ}\text{C}$. A 10 mm/s printing speed was chosen, representing an average value between 9 and 11 mm/s, which have shown the optimal results in the spreading ratio analyses (Figure 1E). According to values calculated by Eq. 2, a higher percentage accuracy (Figure 1F) was observed for both formulations when printed at 15 $^{\circ}\text{C}$, reaching a value of 97% for 3A1M and 91% for 2A2M (Figure 1F). This behavior could be attributed to the higher G' of the blends at 15 $^{\circ}\text{C}$. We hypothesized a higher recovery of collagen triple strands in gelatin at this temperature, resulting in a modification of the hydrogels physico-mechanical properties (Schuurman et al., 2013; Contessi Negrini et al., 2020). On the other hand, according to the results obtained by Eq. 3, a pore factor value closer to 1 was obtained for 3A1M when printed at 15 $^{\circ}\text{C}$, while for 2A2M the value dropped from 0.96 ($T = 25^{\circ}\text{C}$) to 0.93 ($T = 15^{\circ}\text{C}$) (Figure 1G), showing a qualitatively



fractured-like structure of the filament as observed for the 1A3M blend in the filament test. This could be explained by an over-gelated state of the blend, influenced by the gel state of gelatin and a higher MC percentage compared to 3A1M.

3.3 Compressive mechanical properties

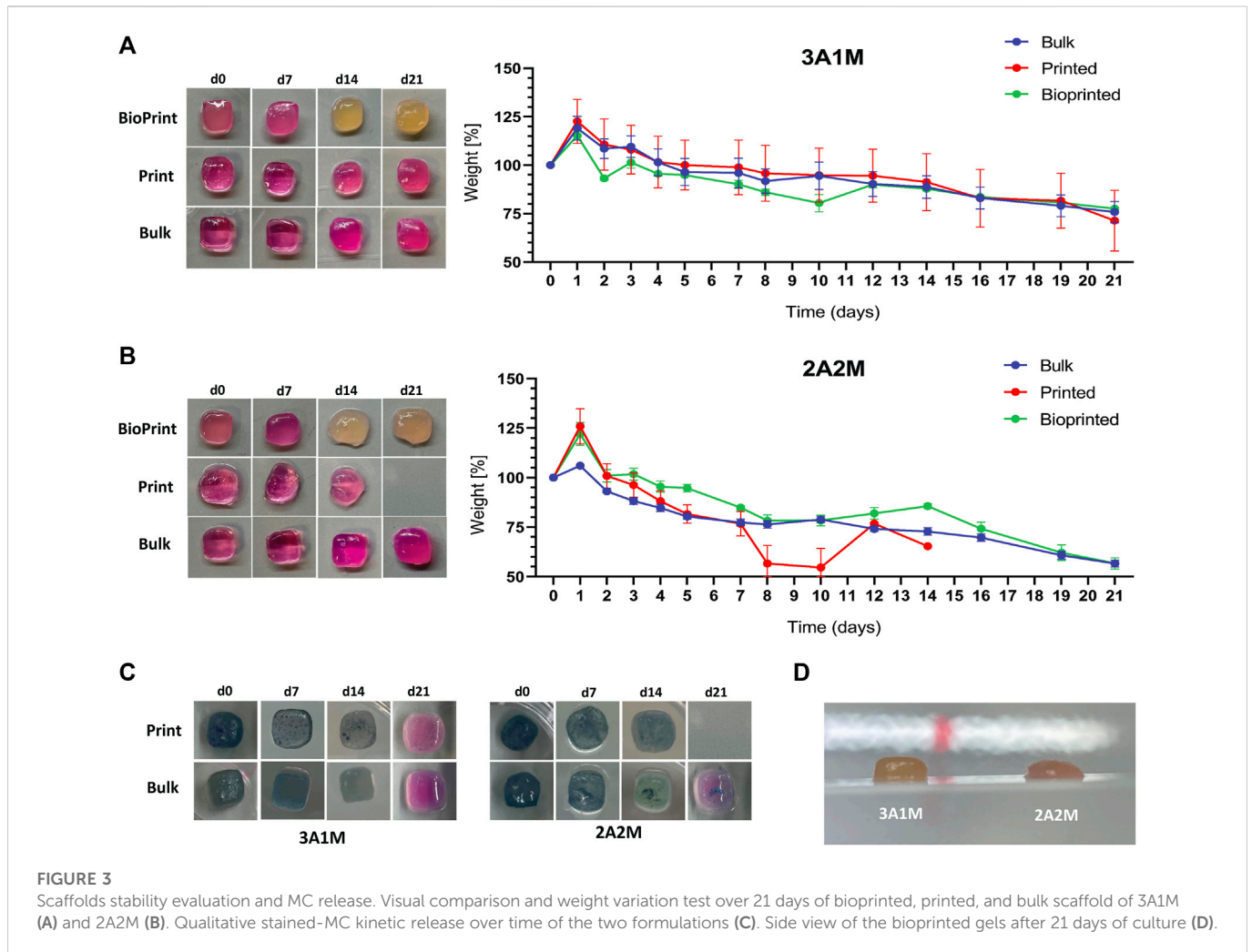
A representative curve of the compressive mechanical properties of the 3A1M and 2A2M blends and the mechanical parameters calculated from stress/strain curves are reported in Figure 2. Both the formulations showed a typical viscoelastic response, characterized by a load curve, where the stress increases with the applied strain during compression, and an unload curve, where the stress decreases (Figure 2A). The viscoelastic behavior was evident by the different response during the load and unload step; in particular, both the formulations exhibited a high hysteresis, evidencing a high contribution of the viscous component of the blends. No significant difference was reported comparing the Young's modulus (E) and the stiffness (K) for the two blends (Figure 2B). Similarly, the maximum stress, representing the stress at the highest compression strain (i.e., 30%), was not statistically different ($p > 0.05$) comparing 3A1M and 2A2M (Figure 2C). The residual strain at the end of the test was similar for the two blends (Figure 2D), evidencing an inhomogeneous behavior

for 2A2M formulation. The same behavior of the two formulations can be attributed to a balancing between the highest Alg concentration in 3A1M and the interaction between Alg, MC, and Gel macromolecules in 2A2M.

3.4 Stability evaluation

The average weight variation of bulk hydrogels during swelling in DMEM culture medium at 37°C is reported in Figure 3. A rapid initial swelling behavior was observed for 3A1M and 2A2M formulations, followed by a gradual weight loss during the incubation time.

Considering the 3A1M, bulk, printed, and bioprinted hydrogels showed a similar trend. At the end of the incubation period ($t = 21$ days) the bulk or printed 3A1M samples qualitatively maintained the original shape (Figure 3A). On the other hand, 2A2M formulation (Figure 3B) showed a greater weight loss ($p < 0.05$) after 21 days compared to 3A1M blend, with a visible shape loss, especially in the bioprinted gels (Figure 3D). In addition, printed 2A2M hydrogels dissolved after 2 weeks in culture condition, whereas 3A1M resulted stable up to 21 days. This behavior could be explained by the higher concentration of Alg in the latter blend, providing a more stable network due to a higher crosslinking density.



Zinc-iodine-chloride was used to stain MC in order to qualitatively observe the kinetic release of methylcellulose from the hydrogels during the incubation for 3 weeks in DMEM culture medium. Results (Figure 3C) showed how the hydrogels stained immediately after preparations (day 0) appeared with dark blue dots, indicating the presence of MC (Schütz et al., 2017). Within 21 days of culture, MC was almost completely released from both bulk and printed 3A1M gels. Contrastingly, a small amount was still visible in 2A2M bulk gels after 3 weeks of incubation in culture medium (Figure 3C). The presence of MC in 2A2M gels after 21 days could be explained by its initial higher quantity in this specific formulation or by weak interactions mediated by weak physical forces among MC and the Alg network (Schütz et al., 2017). Despite the less efficient entrapment of the MC macromolecular chains in the 2A2M blend following Alg crosslinking, MC chains still remain entrapped in the hydrogel bulk at the end of the test.

3.5 Lymphoid cell viability in the hydrogel after 3D bioprinting

MEC1 CLL cell line was initially used (Stacchini et al., 1999) to 3D bioprint the 3A1M and 2A2M formulations. The optimal cell concentration (50×10^6 cells/mL) was selected following our

previous results (Sbrana et al., 2021). Primary peripheral mononuclear cells isolated from buffycoat were subsequently bioprinted using the same procedure. Results from Live/Dead assay performed at different time points qualitatively showed that 3A1M blend kept alive both MEC1 cell line (Figure 4A) and primary cells (Figure 4B) up to 21 days after the bioprinting process, thus proving successful support for lymphoid cells viability. On the other hand, 2A2M bioprinted hydrogels remained stable only for 14 days when MEC1 were embedded, showing faster degradation kinetics compared to 3A1M blend (Figure 4A), probably due to the lower concentration of Alg, therefore a lower crosslinking density. When primary cells were embedded in 2A2M, the samples remained stable for up to 21 days. In parallel for MEC1 cells printed in 3A1M, the formulation showing better results, we performed an additional test to measure cell health and viability by AlamarBlue assay. We observed high viability increasing over time on days 10 and 14 and decreasing only at the last time point on day 21 (Figure 4C).

3.6 Compressive mechanical properties of 3A1M bioprinted constructs

The mechanical properties of the 3A1M formulation bioprinted with the MEC1 cell line were investigated during the culture period of

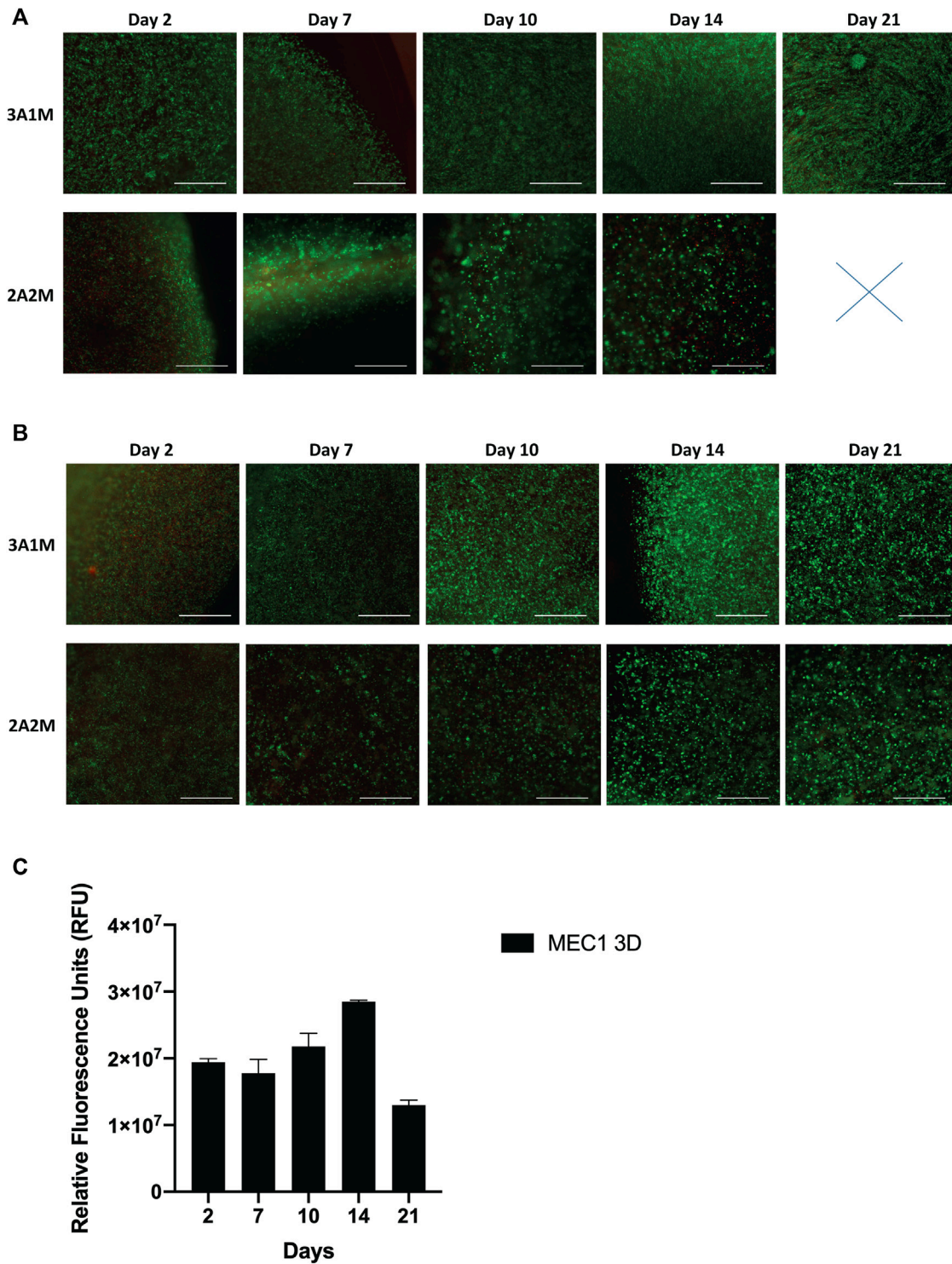


FIGURE 4 Biological characterization of lymphoid cells bioprinted scaffolds. Live/Dead images of bioprinted MEC1 over time of 3A1M and 2A2M (A). Live/Dead images of bioprinted peripheral mononuclear cells over time of 3A1M and 2A2M (B). Scalebar: 200 μ m. (C) AlamarBlue values showing high cell viability in 3A1M mix up to day 14, with subsequent viability drop at day 21.

up to 21 days (Figure 5). At day 0, the Young’s Modulus (E) and stiffness (K) for the bioprinted constructs (Figures 5A, B) showed no significant differences ($p > 0.05$) compared to the printed ones without cells on day 0, indicating how the embedded cells do not alter the mechanical properties of the 3A1M formulation immediately after

printing. However, after the first week of *in vitro* culture, the E and K values dropped and remained lower up to day 21, probably due to the leakage of the Gel and MC macromolecules as previously reported. A spatial rearrangement of the MEC1 within the gel was qualitatively observed through the Live/Dead staining (Figure 5C), probably

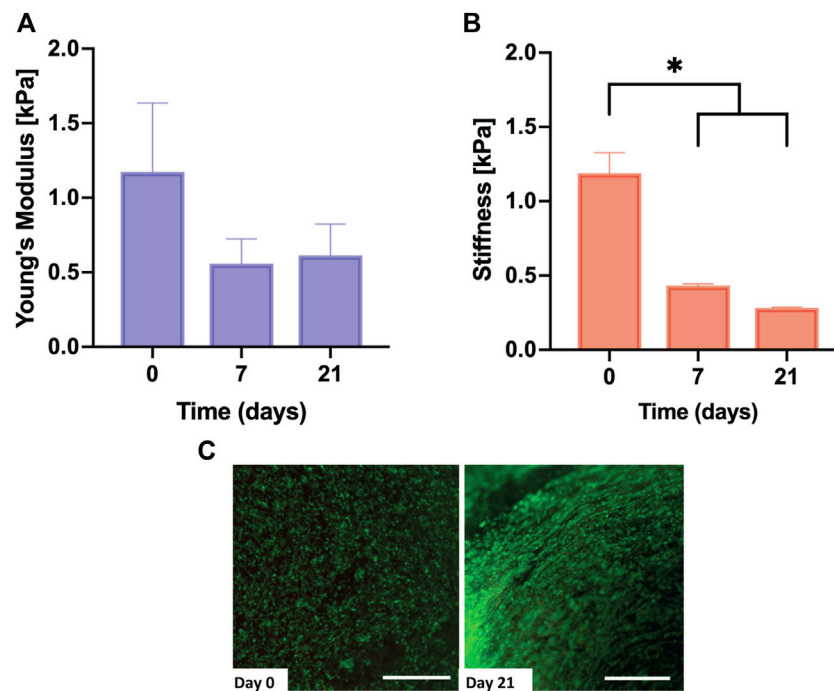


FIGURE 5

Mechanical properties of the bioprinted gels. Young's Modulus (A) and Stiffness (B) of bioprinted 3A1M gels during the culture period (up to 21 days). Live/dead staining of MEC1 cells rearrangement within the bioprinted gel (C). Scale bar: 200 μ m.

enhanced by the movement of the polymer chains, proving how the bioprinted cells experience a 3D mechanically dynamic environment during the culture period.

4 Discussion

In the last years, interest has been raised in the use of 3D bioprinting for pre-clinical applications, in particular for cancer research and the development of new therapies (Mao et al., 2020; Mota et al., 2020; Choi et al., 2021). It is evident and needs to be deeply considered that the tumor microenvironment is different for each type of cell and/or cancer cell, thus it needs a specific and selected bioink to support cell viability and expected cellular behavior. In particular, recapitulating a correct cellular environment mostly depends on the stiffness of the printed or bioprinted ink. We recently demonstrated the feasibility of 3D bioprinting CLL cells (Sbrana et al., 2021) and the necessity to identify a bioink that could better mimic the lymphoid tissue environment.

We here reported the optimization of a new bioink and we demonstrated that it is suitable for the 3D bioprinting of both healthy and leukemic lymphoid cells, possibly thanks to its mechanical properties resembling those of the lymphoid tissues.

To the authors' best knowledge, this work represents the first attempt at developing inks based on Alg, Gel, and MC. An Alg-Gel blend (1.6% w/v Alg, 2% w/v Gel) has already been proposed by Chung et al. (2013) for the development of a bioink containing primary murine myoblasts. Interestingly, at its printing temperature ($T = 5^{\circ}\text{C}$), the Alg-Gel blend displayed G' values (200–300 Pa) comparable with the ones here found for the three formulations in the identified printing temperature range. Furthermore, the formulations here

prepared displayed increased viscoelastic properties as a function of the MC content (0.4%, 0.8%, and 1.2% w/v), in accordance with the literature, where MC has been extensively reported as a thickening additive in MC-alginate blends used both as biomaterial inks and bioinks (Chung et al., 2013; Schütz et al., 2017; Ahlfeld et al., 2020). In this regard, MC-Alg blends have revealed a remarkable potential for the bioprinting of different cell types [e.g., MSCs (Schütz et al., 2017), rat pancreatic islets (Duin et al., 2019), and bovine primary chondrocytes (Hodder et al., 2019)].

The choice to discharge 1A3M formulation was based both on the filament shape after extrusion, resulting rough and unrepeatable, and on the higher pressure needed, which may not adequately preserve suitable cell viability when the hydrogel is used as a bioink (Celikkin et al., 2018; Law et al., 2018). Interestingly, the optimal printing pressure for the selected formulations, i.e., 3A1M and 2A2M ($P = 17$ kPa), resulted even lower than all the printing pressures used by Chung's group ($P = 55, 110, \text{ and } 124$ kPa) for Alg-based inks (Chung et al., 2013).

Compression tests were performed as the mechanical properties of a printed scaffold are pivotal factors influencing its post-printing integrity, and especially the stiffness of the hydrogel can influence the biological behavior of cells (Berridge et al., 2003). In fact, although the importance of the mechanical characteristics of the tumor microenvironment in the proliferation and drug resistance of leukemia cells has been established (Shin and Mooney, 2016), there is still no evidence in the literature on the effect of ECM mechanical parameters on the viability and proliferation of CLL cells. For that reason, in the present work, compressive mechanical tests were performed at 37°C on the printed and bioprinted scaffold at different timepoints. Compression tests did not show any significant difference comparing 3A1M and 2A2M at $t = 0$ (i.e., immediately after

the printing). However, higher stability in time is observed for 3A1M possibly due to the increase in Alg concentration, hence to the higher number of crosslinks and higher chain density (Svozilová et al., 2021). In addition, as demonstrated by Dong et al. (2006) and by Ramesh Babu et al. (2007), interaction among the Alg macromolecules and the ones of Gel and MC have been observed. Interestingly, the stiffness values found for our formulations were in the range found by Shin and Mooney (2016) for hematopoietic tissues.

Since the cancer microenvironment is well-known for its dynamic nature (Datta et al., 2020), recreating a dynamic microenvironment within the printed scaffolds could be a pivotal step in disease recapitulation. For this reason, we performed a stability evaluation and qualitative MC-release kinetic tests. For both 3A1M and 2A2M hydrogels, the initial rapid swelling, followed by a gradual weight loss, could be attributed to the fast dissolution of non-crosslinked Gel from the bulk of the hydrogel. In addition, MC release from the bulk of the hydrogel was in line with the study of Schütz et al. (2017), showing how, for CaCl₂ crosslinked Alg-MC inks, most MC was released within 1 week of incubation. Interestingly, in the present study, MC was still visible in 2A2M ink after 21 days of incubation, probably due to a higher MC presence in 2A2M ink or to the weak interactions among MC and the Alg network.

The two investigated formulations (3A1M and 2A2M) resulted suitable for long-term culture (at least 21 days) of a leukemic cell line, broadly supporting our previous work (Sbrana et al., 2021). In particular, 3A1M formulation was proved to be more stable, resulting in a higher weight % after 21 days of culture, thanks to the higher presence of Alg which increased the crosslinking density and promoted a more stable entrapment of the Gel chains.

The strategy of studying specific tissues related to hematological cancers with 3D *in vitro* models is not largely reported in the scientific literature (Pasikowska et al., 2016; Shin and Mooney, 2016; Scielzo and Ghia, 2020; Svozilová et al., 2021), possibly, due to the circulating nature of the diseases (Calissano et al., 2009; Scarfò et al., 2016). However, leukemic cells in the peripheral blood do not entirely represent the disease, which is composed of lymphoid cells that accumulate and proliferate in the lymphoid tissues (Calissano et al., 2011). Recently, we made the first and only attempt to test whether 3D bioprinting could be applied to model *in vitro* leukemia disease (Sbrana et al., 2021). We proved the feasibility of 3D bioprinting CLL cells and healthy lymphocytes, improving their viability and observing different gene expression profiles, shown by RNAseq analysis, comparing cells cultured in 2D and 3D. In the present study, both healthy lymphoid cells collected from donor peripheral blood and leukemic cells were 3D bioprinted. Live/Dead results confirmed the ones reported in Sbrana et al. (2021), showing that CLL cells were homogeneously distributed in the hydrogels and long-term viability (up to 21 days) was observed. In particular, 3A1M formulation supported the culture for the scheduled time of both cell line and primary cells, due to the higher concentration of Alg, therefore a higher crosslinking density.

The selected 3A1M formulation supported cell viability and the dissolution of the uncrosslinked polymeric chains contributed to cell spatial rearrangement, stimulating them with a 3D mechanically dynamic environment during the culture period. Moreover, the compressive mechanical properties of the gels at the end of the culture period matched the ones of soft lymphoid tissues when tested at 37°C, i.e., physiological condition (Shin and Mooney, 2016; Choi and Harley, 2017).

5 Conclusion

Our work highlights the current need of developing specific bioinks for 3D bioprinting applications different for each cell type. This is becoming central considering the general ambition to recapitulate complex microenvironments using different cell types all at once. In particular, lymphoid cells represent an important target, neglected until now in the field, due to the rapid interest in the development of 3D models to study immune cells in the tumor context. In summary, our work investigated a new bioink able to efficiently support the viability of both CLL cell line and healthy lymphocytes, which can be maintained in culture for up to 21 days, thus supporting the possibility to perform a long-term 3D culture model for leukemia cells. In the future, the complexity of the model can be improved by functionalizing the bioink with specific ECM components and by designing specific geometries to be dynamically cultured. This could allow the design of more accurate lymphoid microenvironment and CLL models in a high throughput process, to test novel drugs such as target therapies or immunotherapy.

Data availability statement

The raw data supporting the conclusion of this article will be made available by the authors, without undue reservation. The data are in repository in the Institutions of the corresponding authors.

Ethics statement

Lymphoid cells were isolated with ficoll gradient from Buffy coats under the approved protocol Leu-Buffy_coat by the Ospedale San Raffaele (OSR, Milan, Italy) ethics committee entitled: "Characterization of leukocyte subpopulations from buffy coats."

Author contributions

SF, CS, DR, and LB wrote the manuscript. CS, DR, RP, FB, MC, and LB performed the experiments and analyzed the data. DR, LB, CS, and SF revised the manuscript. All authors contributed to the article and approved the submitted version.

Funding

The research leading to these results has received funding from: Associazione Italiana per la Ricerca sul Cancro-AIRC under IG 2018-ID. 21332 project-P.I. CS; Leukemia research foundation grant 2018 P.I. CS. Advance Research Grant EHA 2021; Special Program on Metastatic Disease – 5 per mille #2119.

Acknowledgments

We thank Alembic facilities for helpful suggestions and technical support.

Conflict of interest

The authors declare that the research was conducted in the absence of any commercial or financial relationships that could be construed as a potential conflict of interest.

Publisher's note

All claims expressed in this article are solely those of the authors and do not necessarily represent those of their affiliated

organizations, or those of the publisher, the editors and the reviewers. Any product that may be evaluated in this article, or claim that may be made by its manufacturer, is not guaranteed or endorsed by the publisher.

Supplementary material

The Supplementary Material for this article can be found online at: <https://www.frontiersin.org/articles/10.3389/fbiom.2023.1081065/full#supplementary-material>

References

- Ahlfeld, T., Guduric, V., Duin, S., Akkineni, A. R., Schütz, K., Kilian, D., et al. (2020). Methylcellulose – a versatile printing material that enables biofabrication of tissue equivalents with high shape fidelity. *Biomater. Sci.* 8, 2102–2110. doi:10.1039/D0BM00027B
- Ahmed, J. (2017). "Rheological properties of gelatin and advances in measurement," in *Advances in food rheology and its applications* (Elsevier), 377–404. doi:10.1016/B978-0-08-100431-9.00015-2
- Berridge, M. J., Bootman, M. D., and Roderick, H. L. (2003). Calcium signalling: dynamics, homeostasis and remodelling. *Nat. Rev. Mol. Cell Biol.* 4, 517–529. doi:10.1038/nrm1155
- Bonetti, L., De Nardo, L., and Farè, S. (2021). Thermo-responsive methylcellulose hydrogels: From design to applications as smart biomaterials. *Tissue Eng. Part B Rev.* 27, 486–513. doi:10.1089/ten.teb.2020.0202
- Borzacchiello, A., Sala, F. D., and Ambrosio, L. A. (2017). "Rheometry of polymeric biomaterials," in *Characterization of polymeric biomaterials* (Elsevier), 233–253. doi:10.1016/B978-0-08-100737-2.00010-8
- Burger, J. A. (2012). Inhibiting B-cell receptor signaling pathways in chronic lymphocytic leukemia. *Curr. Hematol. Malig. Rep.* 7, 26–33. doi:10.1007/s11899-011-0104-z
- Calissano, C., Damle, R. N., Hayes, G., Murphy, E. J., Hellerstein, M. K., Moreno, C., et al. (2009). *In vivo* intraclonal and interclonal kinetic heterogeneity in B-cell chronic lymphocytic leukemia. *Blood* 114, 4832–4842. doi:10.1182/blood-2009-05-219634
- Calissano, C., Damle, R. N., Marsilio, S., Yan, X.-J., Yancopoulos, S., Hayes, G., et al. (2011). Intraclonal complexity in chronic lymphocytic leukemia: Fractions enriched in recently born/divided and older/quiescent cells. *Mol. Med.* 17, 1374–1382. doi:10.2119/molmed.2011.00360
- Celikkin, N., Simó Padial, J., Costantini, M., Hendrikse, H., Cohn, R., Wilson, C., et al. (2018). 3D printing of thermoresponsive polyisocyanide (PIC) hydrogels as bioink and fugitive material for tissue engineering. *Polym. (Basel)* 10, 555. doi:10.3390/polym10050555
- Choi, J. S., and Harley, B. A. C. (2017). Marrow-inspired matrix cues rapidly affect early fate decisions of hematopoietic stem and progenitor cells. *Sci. Adv.* 3, e1600455. doi:10.1126/sciadv.1600455
- Choi, Y.-J., Park, H., Ha, D.-H., Yun, H.-S., Yi, H.-G., and Lee, H. (2021). 3D bioprinting of *in vitro* models using hydrogel-based bioinks. *Polym. (Basel)* 13, 366. doi:10.3390/polym13030366
- Chung, J. H. Y., Naficy, S., Yue, Z., Kapsa, R., Quigley, A., Moulton, S. E., et al. (2013). Bio-ink properties and printability for extrusion printing living cells. *Biomater. Sci.* 1, 763–773. doi:10.1039/c3bm00012e
- Contessi Negrini, N., Bonetti, L., Contili, L., and Farè, S. (2018). 3D printing of methylcellulose-based hydrogels. *Bioprinting* 10, e00024. doi:10.1016/j.bprint.2018.e00024
- Contessi Negrini, N., Celikkin, N., Tarsini, P., Farè, S., and Świższkowski, W. (2020). Three-dimensional printing of chemically crosslinked gelatin hydrogels for adipose tissue engineering. *Biofabrication* 12, 025001. doi:10.1088/1758-5090/ab56f9
- Coughlin, M. L., Liberman, L., Ertem, S. P., Edmund, J., Bates, F. S., and Lodge, T. P. (2021). Methyl cellulose solutions and gels: fibril formation and gelation properties. *Prog. Polym. Sci.* 112, 101324. doi:10.1016/j.progpolymsci.2020.101324
- Datta, P., Dey, M., Ataie, Z., Unutmaz, D., and Ozbolat, I. T. (2020). 3D bioprinting for reconstituting the cancer microenvironment. *NPJ Precis. Oncol.* 4, 18. doi:10.1038/s41698-020-0121-2
- Desbrières, J., Hirrien, M., and Ross-Murphy, S. B. (2000). Thermogelation of methylcellulose: rheological considerations. *Polym. Guildf.* 41, 2451–2461. doi:10.1016/S0032-3861(99)00413-9
- Dong, Z., Wang, Q., and Du, Y. (2006). Alginate/gelatin blend films and their properties for drug controlled release. *J. Memb. Sci.* 280, 37–44. doi:10.1016/j.memsci.2006.01.002
- Duin, S., Schütz, K., Ahlfeld, T., Lehmann, S., Lode, A., Ludwig, B., et al. (2019). 3D bioprinting of functional islets of langerhans in an alginate/methylcellulose hydrogel blend. *Adv. Healthc. Mater.* 8, 1801631. doi:10.1002/adhm.201801631
- Giuseppe, M. D., Law, N., Webb, B., A Macrae, R., Liew, L. J., Sercombe, T. B., et al. (2018). Mechanical behaviour of alginate-gelatin hydrogels for 3D bioprinting. *J. Mech. Behav. Biomed. Mater.* 79, 150–157. doi:10.1016/j.jmbbm.2017.12.018
- Hodder, E., Duin, S., Kilian, D., Ahlfeld, T., Seidel, J., Nachtigall, C., et al. (2019). Investigating the effect of sterilisation methods on the physical properties and cytocompatibility of methyl cellulose used in combination with alginate for 3D-bioplotting of chondrocytes. *J. Mater. Sci. Mater. Med.* 30, 10. doi:10.1007/s10856-018-6211-9
- Jungst, T., Smolan, W., Schacht, K., Scheibel, T., and Groll, J. (2016). Strategies and molecular design criteria for 3D printable hydrogels. *Chem. Rev.* 116, 1496–1539. doi:10.1021/acs.chemrev.5b00303
- Langer, E. M., Allen-Petersen, B. L., King, S. M., Kendsersky, N. D., Turnidge, M. A., Kuziel, G. M., et al. (2019). Modeling tumor phenotypes *in vitro* with three-dimensional bioprinting. *Cell Rep.* 26, 608–623.e6. doi:10.1016/j.celrep.2018.12.090
- Law, N., Doney, B., Glover, H., Qin, Y., Aman, Z. M., Sercombe, T. B., et al. (2018). Characterisation of hyaluronic acid methylcellulose hydrogels for 3D bioprinting. *J. Mech. Behav. Biomed. Mater.* 77, 389–399. doi:10.1016/j.jmbbm.2017.09.031
- Lee, J., Cuddihy, M. J., and Kotov, N. A. (2008). Three-dimensional cell culture matrices: state of the art. *Tissue Eng. Part B Rev.* 14, 61–86. doi:10.1089/ten.teb.2007.0150
- Levato, R., Jungst, T., Scheuring, R. G., Blunk, T., Groll, J., and Malda, J. (2020). From shape to function: The next step in bioprinting. *Adv. Mater.* 32, 1906423. doi:10.1002/adma.201906423
- Malda, J., Visser, J., Melchels, F. P., Jüngst, T., Hennink, W. E., Dhert, W. J., et al. (2013). 25th anniversary article: Engineering hydrogels for biofabrication. *Adv. Mater.* 25, 5011–5028. doi:10.1002/adma.201302042
- Mao, S., Pang, Y., Liu, T., Shao, Y., He, J., Yang, H., et al. (2020). Bioprinting of *in vitro* tumor models for personalized cancer treatment: a review. *Biofabrication* 12, 042001. doi:10.1088/1758-5090/ab97c0
- Meyvantsson, I., and Beebe, D. J. (2008). Cell culture models in microfluidic systems. *Annu. Rev. Anal. Chem. (Palo Alto Calif)* 1, 423–449. doi:10.1146/annurev.anchem.1.031207.113042
- Moroni, L., Boland, T., Burdick, J. A., De Maria, C., Derby, B., Forgacs, G., et al. (2018). Biofabrication: A guide to technology and terminology. *Trends Biotechnol.* 36, 384–402. doi:10.1016/j.tibtech.2017.10.015
- Mota, C., Camarero-Espinosa, S., Baker, M. B., Wieringa, P., and Moroni, L. (2020). Bioprinting: From tissue and organ development to *in vitro* models. *Chem. Rev.* 120, 10547–10607. doi:10.1021/acs.chemrev.9b00789
- Nasatto, P., Pignon, F., Silveira, J., Duarte, M., Nosedà, M., and Rinaudo, M. (2015). Methylcellulose, a cellulose derivative with original physical properties and extended applications. *Polym. (Basel)* 7, 777–803. doi:10.3390/polym7050777
- O'Connell, C., Ren, J., Pope, L., Li, Y., Mohandas, A., Blanchard, R., et al. (2020). Characterizing bioinks for extrusion bioprinting: Printability and rheology. *Methods Mol. Biol.* 2140, 111–133. doi:10.1007/978-1-0716-0520-2_7
- Ouyang, L., Yao, R., Zhao, Y., and Sun, W. (2016). Effect of bioink properties on printability and cell viability for 3D bioplotting of embryonic stem cells. *Biofabrication* 8, 035020. doi:10.1088/1758-5090/8/3/035020
- Pasikowska, M., Walsby, E., Apollonio, B., Cuthill, K., Phillips, E., Coulter, E., et al. (2016). Phenotype and immune function of lymph node and peripheral blood CLL cells are linked to transendothelial migration. *Blood* 128, 563–573. doi:10.1182/blood-2016-01-683128
- Ramesh Babu, V., Sairam, M., Hosamani, K. M., and Aminabhavi, T. M. (2007). Preparation of sodium alginate–methylcellulose blend microspheres for controlled release of nifedipine. *Carbohydr. Polym.* 69, 241–250. doi:10.1016/j.carbpol.2006.09.027

- Ribeiro, A., Blokzijl, M. M., Levato, R., Visser, C. W., Castilho, M., Hennink, W. E., et al. (2017). Assessing bioink shape fidelity to aid material development in 3D bioprinting. *Biofabrication* 10, 014102. doi:10.1088/1758-5090/aa90e2
- Sbrana, F. V., Pinos, R., Barbaglio, F., Ribezi, D., Scagnoli, F., Scarfò, L., et al. (2021). 3D bioprinting allows the establishment of long-term 3D culture model for chronic lymphocytic leukemia cells. *Front. Immunol.* 12, 639572. doi:10.3389/fimmu.2021.639572
- Scarfò, L., Ferreri, A. J. M., and Ghia, P. (2016). Chronic lymphocytic leukaemia. *Crit. Rev. Oncol. Hematol.* 104, 169–182. doi:10.1016/j.critrevonc.2016.06.003
- Schütz, K., Placht, A.-M., Paul, B., Brüggemeier, S., Gelinsky, M., and Lode, A. (2017). Three-dimensional plotting of a cell-laden alginate/methylcellulose blend: towards biofabrication of tissue engineering constructs with clinically relevant dimensions. *J. Tissue Eng. Regen. Med.* 11, 1574–1587. doi:10.1002/term.2058
- Schuurman, W., Levett, P. A., Pot, M. W., van Weeren, P. R., Dhert, W. J. A., Huttmacher, D. W., et al. (2013). Gelatin-methacrylamide hydrogels as potential biomaterials for fabrication of tissue-engineered cartilage constructs. *Macromol. Biosci.* 13, 551–561. doi:10.1002/mabi.201200471
- Schwab, A., Levato, R., D'Este, M., Piluso, S., Eglin, D., and Malda, J. (2020). Printability and shape fidelity of bioinks in 3D bioprinting. *Chem. Rev.* 120, 11028–11055. doi:10.1021/acs.chemrev.0c00084
- Scielzo, C., and Ghia, P. (2020). Modeling the leukemia microenvironment *in vitro*. *Front. Oncol.* 10, 607608. doi:10.3389/fonc.2020.607608
- Shin, J.-W., and Mooney, D. J. (2016). Extracellular matrix stiffness causes systematic variations in proliferation and chemosensitivity in myeloid leukemias. *Proc. Natl. Acad. Sci.* 113, 12126–12131. doi:10.1073/pnas.1611338113
- Soltan, N., Ning, L., Mohabatpour, F., Papagerakis, P., and Chen, X. (2019). Printability and cell viability in bioprinting alginate dialdehyde-gelatin scaffolds. *ACS Biomater. Sci. Eng.* 5, 2976–2987. doi:10.1021/acsbomaterials.9b00167
- Stacchini, A., Aragno, M., Vallario, A., Alfarano, A., Circosta, P., Gottardi, D., et al. (1999). MEC1 and MEC2: two new cell lines derived from B-chronic lymphocytic leukaemia in prolymphocytoid transformation. *Leuk. Res.* 23, 127–136. doi:10.1016/s0145-2126(98)00154-4
- Svozilová, H., Plichta, Z., Proks, V., Studená, R., Baloun, J., Doubek, M., et al. (2021). RGDS-modified superporous poly(2-hydroxyethyl methacrylate)-based scaffolds as 3D *in vitro* leukemia model. *Int. J. Mol. Sci.* 22, 2376. doi:10.3390/ijms22052376
- Thayer, P., Martinez, H., and Gatenholm, E. (2020). History and trends of 3D bioprinting. *Methods Mol. Biol.* 2140, 3–18. doi:10.1007/978-1-0716-0520-2_1
- Van Hoorick, J., Declercq, H., De Muynck, A., Houben, A., Van Hoorebeke, L., Cornelissen, R., et al. (2015). Indirect additive manufacturing as an elegant tool for the production of self-supporting low density gelatin scaffolds. *J. Mater. Sci. Mater. Med.* 26, 247. doi:10.1007/s10856-015-5566-4
- Yamada, K. M., and Cukierman, E. (2007). Modeling tissue morphogenesis and cancer in 3D. *Cell* 130, 601–610. doi:10.1016/j.cell.2007.08.006
- Young, E. W., and Beebe, D. J. (2010). Fundamentals of microfluidic cell culture in controlled microenvironments. *Chem. Soc. Rev.* 39, 1036–1048. doi:10.1039/b909900j